Optical Materials 46 (2015) 34–39

Contents lists available at ScienceDirect

Optical Materials

journal homepage: www.elsevier.com/locate/optmat

# Spectroscopic properties of $Eu^{3+}/Nd^{3+}$ co-doped phosphate glasses and opaque glass–ceramics

R. Narro-García [a,*], H. Desirena [b], T. López-Luke [b], J. Guerrero-Contreras [c], C.K. Jayasankar [d], R. Quintero-Torres [a], E. De la Rosa [b]

[a] Centro de Física Aplicada y Tecnología Avanzada, Universidad Nacional Autónoma de México, Boulevard Juriquilla 3001, Querétaro 76230, Querétaro, Mexico
[b] Centro de Investigaciones en Óptica, A.P. 1-948, León, Gto 37150, Mexico
[c] Instituto Politécnico Nacional, CICATA-Unidad Altamira, Tamaulipas 89600, Mexico
[d] Department of Physics, Sri Venkateswara University, Tirupati 517502, India

ARTICLE INFO

*Article history:*
Received 12 February 2015
Received in revised form 29 March 2015
Accepted 30 March 2015
Available online 23 April 2015

*Keywords:*
$Eu^{3+}/Nd^{3+}$ co-doped glasses
Phosphate glasses
Glass–ceramics
Opaque glass–ceramics

ABSTRACT

This paper reports the fabrication and characterization of $Eu^{3+}/Nd^{3+}$ co-doped phosphate (PNE) glasses and glass–ceramics as a function of $Eu^{3+}$ concentration. The precursor glasses were prepared by the conventional melt quenching technique and the opaque glass–ceramics were obtained by heating the precursor glasses at 450 °C for 30 h. The structural and optical properties of the glass and glass–ceramics were analyzed by means of X-ray diffraction, Raman spectroscopy, UV–VIS–IR absorption spectroscopy, photoluminescence spectra and lifetimes. The amorphous and crystalline structures of the precursor glass and opaque glass–ceramic were confirmed by X-ray diffraction respectively. The Raman spectra showed that the maximum phonon energy decreased from 1317 $cm^{-1}$ to 1277 $cm^{-1}$ with the thermal treatment. The luminescence spectra of the glass and glass–ceramic samples were studied under 396 nm and 806 nm excitation. The emission intensity of the bands observed in opaque glass–ceramic is stronger than that of the precursor glass. The luminescence spectra show strong dependence on the $Eu^{3+}$ ion concentration in the $Nd^{3+}$ ion photoluminescence (PL) intensity, which suggest the presence of energy transfer (ET) and cross-relaxation (CR) processes. The lifetimes of the $^4F_{3/2}$ state of $Nd^{3+}$ ion in $Eu^{3+}/Nd^{3+}$ co-doped phosphate glasses and glass–ceramics under 806 nm excitation were measured. It was observed that the lifetimes of the $^4F_{3/2}$ level of $Nd^{3+}$ of both glasses and glass–ceramics decrease with the increasing $Eu^{3+}$ concentration. However in the case of opaque glass–ceramics the lifetimes decrease only 16%.



## 1. Introduction

Glass–ceramics are one of the relatively new members of the ceramics' family and an important electroceramic type. These materials are obtained from a glass by suitable heat treatments, with the objective to produce the nucleation and growth of certain crystalline phases that are immersed in the residual vitreous matrix [1]. The advantage that a glass–ceramic offers over either glass or ceramic materials is the combination of easy fabrication and outstanding mechanical properties. Since glass–ceramic matrix have zero porosity and submicron grains, they are mechanically stronger than many conventional glass and ceramic matrix [2].

Glass–ceramics could be classified in transparent or opaque glass–ceramic depending on their transmittance, which depends in a sensitive way on the annealing condition used to induce crystallization [3].

Transparent glass–ceramic as host materials for active optical ions have attracted great interest recently due to their potential application in optical devices such as frequency-conversion materials [4,5], lasers [6,7] and optical fiber amplifiers [8–11]. It have been demonstrated that the rare-earth doped transparent glass–ceramics, in which rare-earth ions selectively incorporated into the crystalline phase, may combine the favorable properties such as low phonon energy, high mechanical and chemical stabilities in glass matrix similar to crystalline environment [12,13].

On the other hand, little research has been done in the field of opaque glass–ceramics doped with rare-earths [14–16]. Pie et al. [17] showed that the photo-stimulated luminescence in Eu-doped

* Corresponding author.
*E-mail address:* roberto.narro@gmail.com (R. Narro-García).

http://dx.doi.org/10.1016/j.optmat.2015.03.051
0925-3467/

fluorochlorozirconate opaque glass–ceramic is stronger than in glass or transparent glass–ceramic. This was due to an increasing volume fraction of orthorhombic $BaCl_2$. In addition, opaque glass–ceramics show good chemical durability, mechanical strength, and corrosion resistance. Based on this point, opaque glass–ceramics are more competitive than glasses in the development of white lighting, sensor and planar medical display devices. Hence, further attempts at developing rare-earth doped opaque glass–ceramics have important significance in the development of luminescent materials.

In the present work we introduce a new glass and glass–ceramic matrix based on Sodium Phosphate ($NaH_2P_2O_5H_2O$) which is one the best host for photonic applications with high rare earth elements solubility without ion cluster formation [18]. This fact is due to large amount of non-bridging oxygen [19]. With the aim to improve the thermal and mechanical properties of the host, Aluminum Oxide ($Al_2O_3$) and Barium Oxide (BaO) were added, respectively [20–22]. On the other hand, in order to decrease the melt temperature, improving the rare earth elements solubility by creating new non-bridging oxygen, reducing the water content and promoting the removal of bubbles, Potassium Carbonate ($K_2CO_3$) and Sodium Fluoride (NaF) were added, respectively [23]. Finally, Lanthanum Oxide ($La_2O_3$) which has an ionic radius similar to the rare earths was added to the host composition for substitution of rare earths without modifying the glass composition.

The motive of the present study is to investigate the optical properties of $Eu^{3+}/Nd^{3+}$ co-doped phosphate (PNE) glasses and opaque glass–ceramics. The precipitation of crystallites and the incorporation of $Eu^{3+}$ and $Nd^{3+}$ into the crystallites were confirmed by X-ray diffraction, Raman spectroscopy and photoluminescence spectra. The luminescence spectra of the glass and glass–ceramic samples were studied under 396 nm and 806 nm excitation.

## 2. Experimental

### 2.1. Sample preparation

All samples were prepared from the starting chemical constituent sodium phosphate ($NaH_2P_2O_5H_2O$), aluminum oxide ($Al_2O_3$), barium oxide (BaO), potassium carbonate ($K_2CO_3$), sodium fluoride (NaF), europium oxide ($Eu_2O_3$), neodymium oxide ($Nd_2O_3$) and lanthanum oxide ($La_2O_3$). The glass composition was $66P_2O_5$–$10.5Al_2O_3$–3.05BaO–$16.5K_2CO_3$–0.7NaF–$xEu_2O_3$–$0.5Nd_2O_3$–$(2.75-x)$ $La_2O_3$ (mol.%), where $x = 0$, 0.25, 0.5, 0.75, 1.5 and 2 referred as PNE-0, PNE-0.25, PNE-0.5, PNE-0.75, PNE-1.5 and PNE-2, respectively. Calculated quantities of precursors were mixed in a glass dish and melted in an electric furnace at 1200 °C for 3 h in a platinum crucible so that a homogeneously mixed melt was obtained. The melt was cast into a suitable aluminum mold kept at 400 °C. The obtained glasses were subsequently annealed at 400 °C for 18 h. The annealing process sought to minimize the internal mechanical stress to obtain glasses with good mechanical stability. The glass samples were polished to optical quality and only bubble and streak free samples were taken for optical measurements. Samples were cut and polished to 2 mm thick slabs for different measurements. Finally, the opaque glass–ceramic samples were prepared by heating the $Eu^{3+}/Nd^{3+}$ co-doped phosphate glasses at 450 °C for 30 h (temperature between the glass transition and crystallization temperatures). Fig. 1 shows a photograph of the glass and opaque glass–ceramic samples before and after thermal treatment, respectively. It is observed that the obtained glass–ceramics have a milky appearance caused by the formation of small crystallites inside the glass.


**Fig. 1.** Photograph of the glass (left sample) and opaque glass–ceramic (right sample).

### 2.2. Structural and optical characterization

The X-ray diffraction (XRD) patterns were obtained using SIEMENSD-5005 equipment provided with a Cu tube with Kα radiation at 1.5405 Å, scanning in the 15–100°, $2\theta$ range with increments of 0.02° and a swept time of 8 s. The Raman signals were collected using a Renishaw Raman System (Renishaw Inc., model RM2000) with a 20× objective lens in backscattering geometry. The excitation laser wavelength was 514 nm. The integration time for each Raman measurement was 30 s. The UV–VIS–NIR absorbance spectra (350–930 nm) of the PNE glass samples were measured with a spectrometer (Perkin Elmer Lamda 900) with 1 nm resolution. The photoluminescence (PL) spectra were recorded by exciting the samples with two different excitation sources: a xenon arc lamp and a continuous wave laser diode centered at the wavelength of 396 nm and 806 nm, respectively. The emitted signal was focused onto a PC-controlled SP-2357 spectrograph (Acton Research) and detected by a photomultiplier tube R955 (Hamamatsu) and InGaAs detector (Thorlabs DET10C). The system was controlled with a PC where PL spectra were obtained. Fluorescence lifetime was measured using a pulsed laser diode with a monochromator and InGaAs detector connected to a Tektronix Oscilloscope. All the measurements were performed at room temperature.

## 3. Results and discussion

### 3.1. XRD patterns

The representative XRD patterns for the precursor glass and glass–ceramic are shown in Fig. 2. For the precursor glass, an amorphous structure is observed. For the glass–ceramic, seven crystalline structures were formed (1) potassium barium phosphate (PBP: $KBa_2(PO_3)_5$), (2) barium phosphide (BP: $Ba_5P_9$), (3) barium neodymium oxide (BNO: $BaNd_2O_4$), (4) potassium phosphorous fluoride (KPF: $K(PF_6)$), barium aluminum fluoride (BAlF: $Ba(AlF_5)$), (6) sodium barium phosphate (NaBP: $Na_4Ba(PO_3)_6$) and aluminum phosphate (AlP: $AlPO_4$). The peaks at 25.681°, 26.550°, 26.209°, 26.758° and 27.643° correspond to PBP planes of (120), (202), (−112), (−301), and (310), respectively, indexed to JCPDS No. 00-036-1478. The peaks at 30.225°, 30.398°, 25.653° and 22.745°, correspond to BP planes of (422), (351), (151) and (440), respectively, indexed to JCPDS No. 01-074-3523. The peaks at 29.070°, 28.679° and 33.988° correspond to BNO planes of (302), (004) and (112), respectively, indexed to JCPDS No. 01-086-0678. The peaks at 25.157°, 29.337°, 46.996° and 19.226° correspond to KPF planes of (110), (012), (21−2) and (101), respectively, indexed

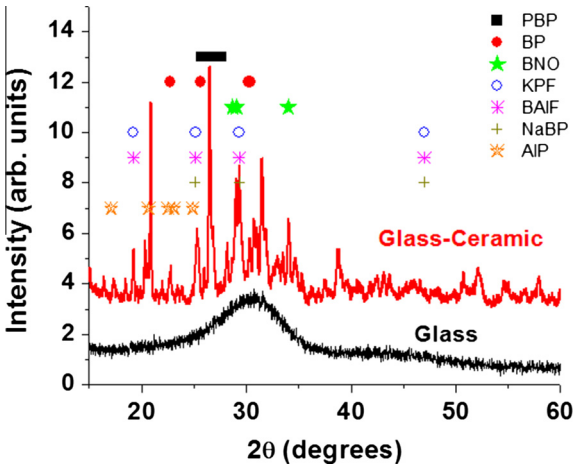


**Fig. 2.** XRD patterns of the precursor glass and glass–ceramic. Seven crystalline structures were formed: potassium barium phosphate (PBP), barium phosphide (BP), barium neodymium oxide (BNO), potassium phosphorous fluoride (KPF), barium aluminum fluoride (BAlF), sodium barium phosphate (NaBP) and aluminum phosphate (AlP).

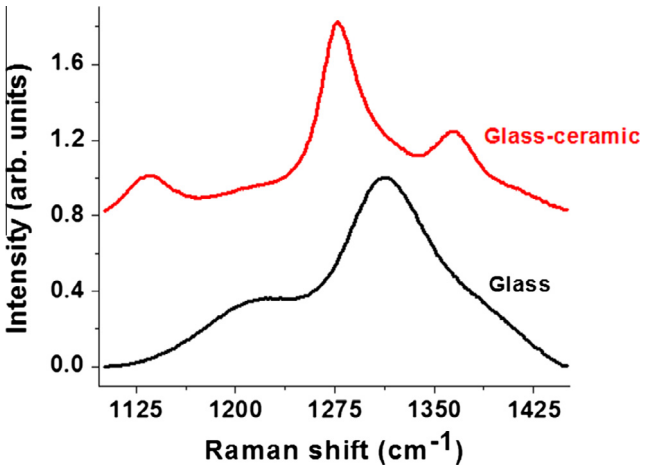


**Fig. 3.** Raman spectra of the precursor glass and glass–ceramic.

according to JCPDS No. 01-071-5014. The peaks at 25.259°, 24.579°, 23.509°, 22.538° and 34.393° correspond to BAlF planes of (−1−12), (103), (−112), (1−1−1) and (1−22), respectively, indexed according to JCPDS No. 01-071-2941. The peaks at 30.412°, 34.706° and 23.952 correspond to NaBP planes of (2−21), (−130) and (211), respectively, indexed to JCPDS No. 00-038-1469. The relevance of these observations is important in two directions; on one hand is to emphasize the remarkable transformation in the material structure with the annealing at 450 °C, and on the other hand, the different crystalline structures presented in the opaque glass–ceramic could change the local environment of the active $Nd^{+3}$ and $Eu^{+3}$ ions. The later may justifies the change in photoluminescence as has been shown by [13] and discussed in the photoluminescence spectra Section 3.4.

### 3.2. Raman spectra

Additional evidence for the structure of the glass and glass–ceramic comes from their Raman spectra as shown in Fig. 3. Raman spectrum of the glass shows two peaks at 1215 and 1317 $cm^{-1}$. The glass–ceramic shows three well defined peaks at 1138, 1277 and 1367 $cm^{-1}$. The principal Raman stretching vibration is due to phosphorus compounds (P═O), which results in a band between 1350 and 1140 $cm^{-1}$ [24]. This result agrees with the results of XRD, which showed that the glass–ceramic presents different phases combined with phosphorus–oxygen. Another important point observed from Fig. 3 is that the maximum phonon energy decreased from 1317 $cm^{-1}$ to 1277 $cm^{-1}$ with the thermal treatment which could be explained by the formation of multiple crystalline phases inside the glass–ceramic (see Fig. 2). In addition to the publish results [25] that indicates the correlation between Raman stretching wavenumbers of phosphorus–oxygen bonds and their bond lengths in inorganic crystalline phosphates and its consequences in other physical variables. The sharper peaks in the Raman signal for the glass–ceramic samples gives evidence toward precise definition of the vibrational states used in Fig. 7. The access to these vibrations increases the probability for radiative recombination, hence increasing the photoluminescence. Also it is observed a decrease in the integrated Raman intensity with the glass–ceramic formation. This decrease in the integrated Raman intensity is associated with an enlargement in the photoluminescence, a trend also observed in other systems [26].

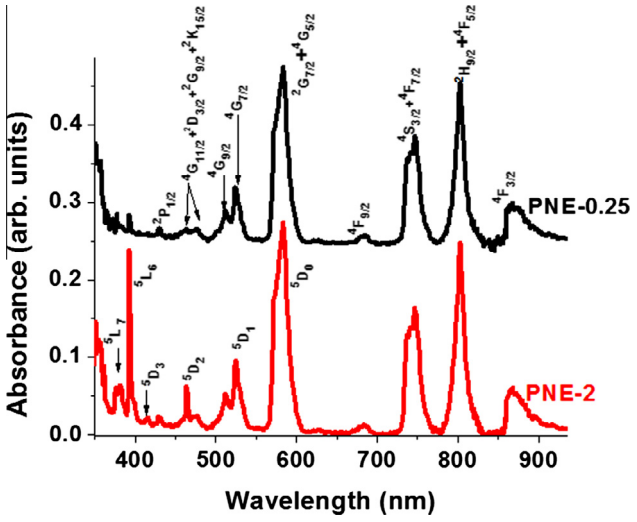


**Fig. 4.** Optical absorption spectra of $Eu^{3+}/Nd^{3+}$ co-doped phosphate glasses.

### 3.3. Absorption spectra

Fig. 4 shows the UV–Vis–NIR absorption spectra of $Eu^{3+}/Nd^{3+}$ co-doped phosphate (PNE) glasses. The absorption spectrum of PNE-0.25 glass network with low $Eu^{3+}$ ion concentration shows strong absorption bands at 430, 477, 512, 526, 583, 685, 747, 803 and 868 nm in the range of 350–950 nm which correspond to $Nd^{3+}$ ion originating from the ground $^4I_{9/2}$ level to number of closely spaced higher energy levels and are assigned to as $^4I_{9/2} \rightarrow {}^2P_{1/2}$, $^4G_{11/2} + {}^2D_{3/2} + {}^2G_{9/2} + {}^2K_{15/2}$, $^4G_{9/2}$, $^4G_{7/2}$, $^2G_{7/2} + {}^4G_{5/2}$, $^4F_{9/2}$, $^4S_{3/2} + {}^4F_{7/2}$, $^2H_{9/2} + {}^4F_{5/2}$ and $^4F_{3/2}$ transitions, respectively [27]. In the case of the absorption spectrum of PNE-2 sample which has high $Eu^{3+}$ ion concentration shows more intense bands at around 382, 393, 416, 464, 525 and 583 nm; which are attributed to the transitions of $Eu^{3+}$ ions correspond to $^7F_0 \rightarrow {}^5L_7, {}^5L_6, {}^5D_3, {}^5D_2$, $^5D_1$ and $^5D_0$, respectively [28].

### 3.4. Photoluminescence spectra

$Eu^{3+}$ ions in PNE glasses and glass–ceramics emit red[1] color under 396 nm excitation, such emission is strong that could be seen with naked eye. Fig. 5 shows the photoluminescence (PL) spectra of

[1] For interpretation of color in Fig. 4, the reader is referred to the web version of this article.

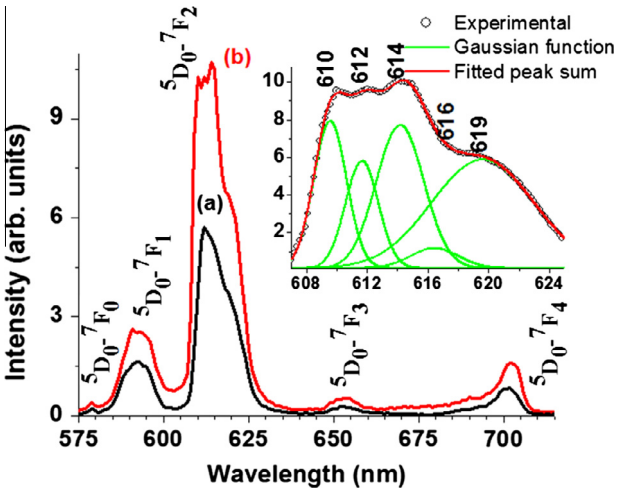


**Fig. 5.** PL spectra of PNE-1.5 glass (a) and glass–ceramic (b) under 396 nm excitation, measured at room temperature. The inset indicates the sharp peaks of glass–ceramic around 612 nm.

the PNE-1.5 glass and glass–ceramic under 396 nm excitation in the wavelength range of 575–715 nm. Each PL spectrum consists of 5 PL bands corresponding to $^5D_0 \rightarrow {}^7F_J$ ($J = 0$–4) transitions of $Eu^{3+}$ ions. The strongest band centered at 612 nm corresponds to $^5D_0 \rightarrow {}^7F_2$ transition. This band is attributed to the forced electric-dipole transition allowed only at low symmetries with no inversion center which is also hypersensitive transition and found to be very sensitive to the local structure surrounding the $Eu^{3+}$ ions [29]. There are three notable differences in the PL spectrum of PNE-1.5 glass compared to the PL spectrum of PNE-1.5 glass–ceramic. First, the glass–ceramic spectrum for $^5D_0 \rightarrow {}^7F_2$ transition shows 5 peaks located at 610, 612, 614, 616 and 619 nm (see the inset of Fig. 5). This behavior is related mainly to the Stark effect which tends to raise the degeneracy of $^7F_J$ levels involved in the glass–ceramics transitions [16]. Second, the asymmetry ratio ($R$) defined as $R = (^5D_0 \rightarrow {}^7F_2)/(^5D_0 \rightarrow {}^7F_1)$ calculated from the PL spectrum of the glass–ceramic ($R_{GC} = 4.72$) is higher than the $R$ calculated from the PL spectrum of the glass ($R_G = 3.72$). The $R$ provides a measure of the degree of distortion of the inversion symmetry of the local $Eu^{3+}$ ions in the lattice [30]. If the $R$ value is low, the $Eu^{3+}$ tends to localize at a high symmetry site or centrosymmetric site. In contrast when the $R$ value is high, the $Eu^{3+}$ tends to localize at a low symmetry site or non-centrosymmetric site. The latter suggests, a change in the local structure surrounding the $Eu^{3+}$ ions due to the thermal treatment and that the $Eu^{3+}$ ions in the glass–ceramic tends to localize at a low symmetry site or non-centrosymmetric site. Third, the PL intensity of the glass–ceramic is stronger compared to those of the precursor glass. The overall intensity (defined as the sum of the area under the curve of the $^5D_0 \rightarrow {}^7F_J$ transitions) is 1.8 times bigger than the precursor glass. The enhancement of PL intensity in glass–ceramic can be explained by the phonon energy of the host lattice. $Eu^{3+}$ ions from $^5D_{1,2}$ to $^7F_J$ ($J = 0,1,2,3,4$) transitions depend critically on the dominant vibration frequencies available of the host lattice. If the maximum phonon energy of the host lattice is large enough, the population of $Eu^{3+}$ ions at $^5D_{1,2}$ excited state may be depleted through nonradiative multiphonon relaxation. The lower the maximum phonon energy of the host matrix, the lower the multiphonon relaxation probability. According to the Raman spectra the maximum phonon energy decreased from 1317 $cm^{-1}$ to 1277 $cm^{-1}$ with the thermal treatment. Therefore, the enhancement of PL intensity in glass–ceramic indicates the presence of $Eu^{3+}$ ions in low phonon energy crystallites [13].

It is well known that energy transfer (ET) process can only occur if the energy differences between the ground and excited states of sensitizer and activator are equal (resonance condition) and if a suitable interaction between both systems exists. According to Dieke diagram this resonance condition is satisfied for the $^5D_0 \rightarrow {}^7F_1(Eu^{3+})$ and $^4I_{9/2} \rightarrow (^2G_{7/2} + {}^4G_{5/2})$ ($Nd^{3+}$) transitions. Fig. 6(a) shows the infrared PL spectra of the PNE-1.5 glass and glass–ceramic under 396 nm excitation. Each PL spectrum consists of 3 photoluminescence bands centered at 875, 1052 and 1324 nm, which are assigned to the $^4F_{3/2} \rightarrow {}^4I_{9/2}$, $^4I_{11/2}$ and $^4I_{13/2}$ transitions of

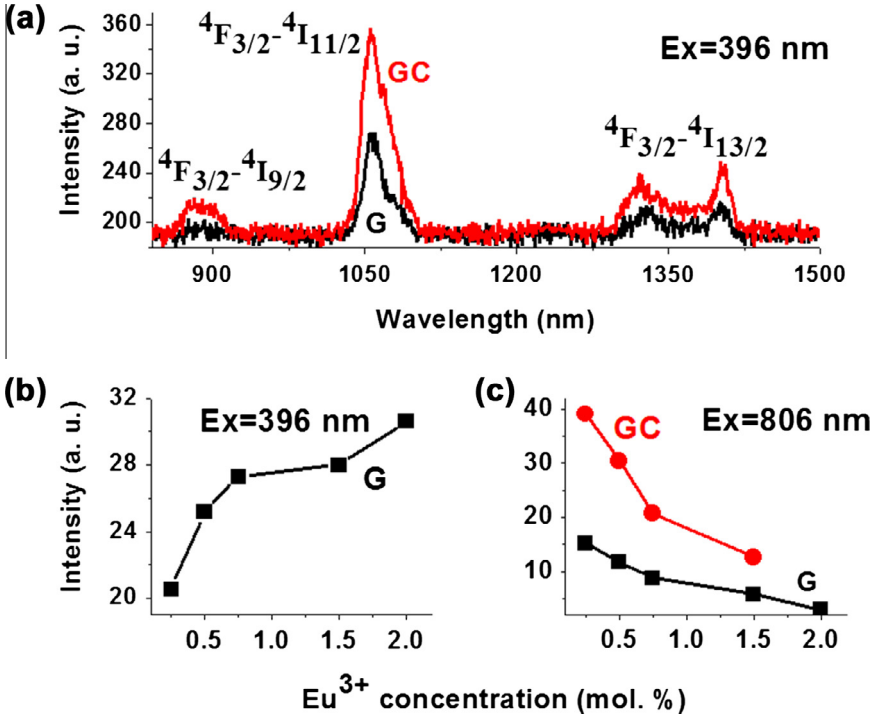


**Fig. 6.** (a) PL spectra of PNE-1.5 glass (G) and glass–ceramic (GC) under 396 nm excitation. Intensity at 1057 nm as a function of $Eu^{3+}$ concentration in $Eu^{3+}/Nd^{3+}$ co-doped phosphate glasses and glass–ceramics under 396 nm (b) and 806 nm (c) excitation.

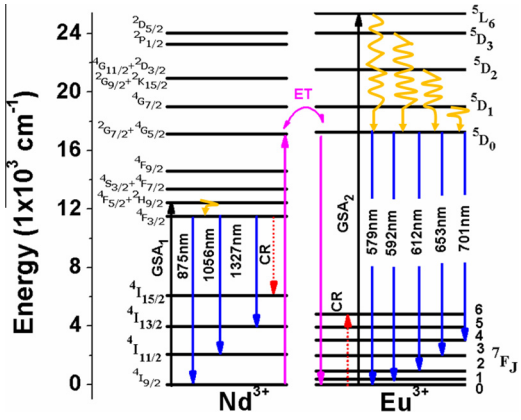


**Fig. 7.** Energy level diagram of $Nd^{3+}$ and $Eu^{3+}$ ions showing the ground state absorption (GSA), the cross-relaxation process (CR) and the energy transfer (ET) process.

$Nd^{3+}$, respectively. Although no distinct difference in peak position and width was observed for $^4F_{3/2} \rightarrow {}^4I_{11/2}$ transition, PL intensity of glass–ceramic was stronger than that of the precursor glass. The enhancement of fluorescence intensity in glass–ceramic is due to the incorporation of $Nd^{3+}$ into crystalline phase with lower phonon energy, which agrees with Ref. [12].

Moreover, it was observed that the intensity of $Nd^{3+}$ emission increased with increasing of $Eu^{3+}$ concentration under 396 nm excitation in the PNE glasses (see Fig. 6(b)). This result could evidently indicate the existence of an ET process between the $Eu^{3+}$ and $Nd^{3+}$ ions as follow: $^5D_0$ $(Eu^{3+}) + {}^4I_{9/2}(Nd^{3+}) \rightarrow {}^7F_1(Eu^{3+}) + ({}^2G_{7/2} + {}^4G_{5/2})$ $(Nd^{3+})$ (see Fig. 7).

However, experimental results suggest the presence of an additional quenching process from $Nd^{3+}$ to $Eu^{3+}$ ions. For example, the variation of luminescence intensity of the transition centered at 1061 nm $({}^4F_{3/2} \rightarrow {}^4I_{11/2})$ with $Eu^{3+}$ ion concentration under 806 nm is depicted in Fig. 6(c). The decrease of this band with the $Eu^{3+}$ ion concentration may be attributed to the cross relaxation process $({}^4F_{3/2} + {}^7F_0) \rightarrow ({}^4I_{15/2} + {}^7F_6)$ from $Nd^{3+}$ to $Eu^{3+}$ ions as already observed [31,32] (see Fig. 7).

### 3.5. Lifetime measurements

Fig. 8 presents the lifetime values of the $^4F_{3/2} \rightarrow {}^4I_{11/2}$ transition of $Nd^{3+}$ ion at 1056 nm. The lifetimes were measured under

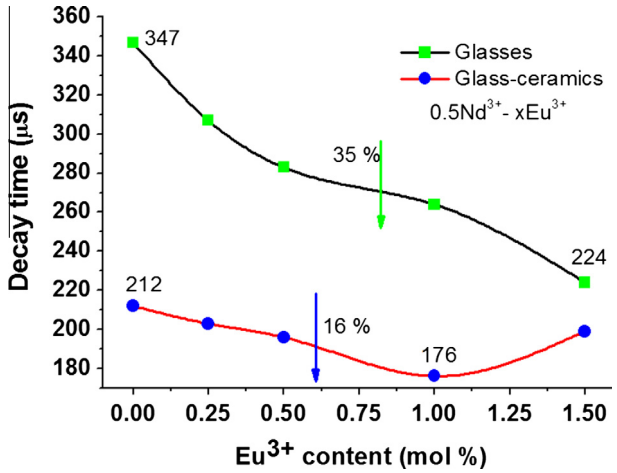


**Fig. 8.** Fluorescence lifetime of the $^4F_{3/2}$ state of $Nd^{3+}$ ion in $Eu^{3+}/Nd^{3+}$ co-doped phosphate glasses and glass–ceramics under 806 nm excitation. The average standard deviation of the lifetime values is around ±3 μs.

806 nm excitation. It was observed that the lifetime of the $^4F_{3/2}$ level of $Nd^{3+}$ decreases with the increasing $Eu^{3+}$ concentration. For example, the glasses lifetime decreased 35% from 347 μs to 207 μs when $Eu^{3+}$ concentration increased from 0 to 2 mol.%. This result confirms that, the $Eu^{3+}$ concentration dependent quenching of $Nd^{3+}$ fluorescence is due to unwanted CR $({}^4F_{3/2} + {}^7F_0) \rightarrow ({}^4I_{15/2} + {}^7F_6)$ between the two ion species, as indicated in Fig. 7. These CR process limit the attractiveness of $Eu^{3+}$ sensitization for $Nd^{3+}$ emission. However, glass–ceramics lifetime decreased only 16% from 212 μs to 176 μs. This result indicates a decrease in the CR process in the case of the glass–ceramics.

## 4. Conclusions

Different concentrations of $Eu^{3+}/Nd^{3+}$ co-doped phosphate glasses and glass–ceramics were prepared by melt quenching method and characterized through XRD, Raman, photoluminescence and lifetime measurements. Multiple crystalline phases were successfully precipitated in the PNE glass–ceramics base glass after thermal treatment. The obtained glass–ceramics have a milky appearance caused by the formation of small crystallites inside the glass. The PL results under UV excitation confirm the existence of an energy transfer process from $Eu^{3+}$ to $Nd^{3+}$. However, when the PNE glasses and glass–ceramics were pumped at 806 nm, it was observed that the infrared PL bands (at 875, 1056 and 1327 nm) of $Nd^{3+}$ ion decreased with increasing the concentration of $Eu^{3+}$ which may be attributed to the presence of an additional CR process $({}^4F_{3/2} + {}^7F_0) \rightarrow ({}^4I_{15/2} + {}^7F_6)$ from $Nd^{3+}$ to $Eu^{3+}$ ions.

It was observed an increase in the PL intensity in both visible and infrared region in the case of glass–ceramics (1.8 times bigger than the precursor glass). The latter, suggest that these opaque glass–ceramics are more competitive than the PNE base glasses in terms of their PL properties.

## Acknowledgements

The authors would like to thank CONACYT for their financial support through grant 134111, Indo-Mexico project 164373. Additionally, authors would like to thank UNAM for postdoctoral scholarship to R. Narro-García.

## References

[1] B.M. Caruta, Ceramics and Composite Materials: New Research, Nova Science Publishers Inc., New York, USA, 2006.
[2] C.A. Harper, Handbook Ceramics, Glasses, and Diamonds, McGraw-Hill, USA, 2001.
[3] A. Edgar, G.V.M. Williams, M. Secu, S. Schweizer, J.M. Spaeth, Optical properties of a high-efficiency glass ceramic X-ray storage phosphor, Radiat. Meas. 38 (2004) 413–416.
[4] Y. Kawamoto, R. Kanno, J. Qiu, Upconversion luminescence of $Er^{3+}$ in transparent $SiO_2$—$PbF_2$—$ErF_3$ glass–ceramics, J. Mater. Sci. 33 (1998) 63–67.
[5] Y. Hatefi, N. Shahtahmasebi, A. Moghimi, E. Attaran, Ultraviolet to visible frequency-conversion properties of rare earths doped glass–ceramics, J. Rare Earths 29 (2011) 484–488.
[6] J. Pisarska, W. Ryba-Romanowski, G. Dominiak-Dzik, T. Goryczka, W.A. Pisarski, Nd-doped oxyfluoroborate glasses and glass–ceramics for NIR laser applications, J. Alloy. Compd. 451 (2008) 223–225.
[7] J. Xie, Q. Zhang, Y. Zhuang, X. Liu, M. Guan, B. Zhu, R. Yang, J. Qiu, Enhanced mid-IR emission in $Yb^{3+}$–$Tm^{3+}$ co-doped oxyfluoride glass–ceramics, J. Alloy. Compd. 509 (2011) 3032–3037.
[8] X. Yu, L. Duan, L. Ni, Z. Wang, Fabrication and luminescence behavior of phosphate glass–ceramics co-doped with $Er^{3+}$ and $Yb^{3+}$, Opt. Commun. 285 (2012) 3805–3808.
[9] E. Augustyn, M. Żelechower, D. Stróż, J. Chrapoński, The microstructure of erbium–ytterbium co-doped oxyfluoride glass–ceramic optical fibers, Opt. Mater. 34 (2012) 944–950.
[10] R. Lisiecki, E. Augustyn, W. Ryba-Romanowski, M. Żelechower, Er-doped and Er, Yb co-doped oxyfluoride glasses and glass–ceramics, structural and optical properties, Opt. Mater. 33 (2011) 1630–1637.
[11] Y. Yu, D. Chen, Y. Wang, F. Liu, E. Ma, A new transparent oxyfluoride glass ceramic with improved luminescence, J. Non-Cryst. Solids 353 (2007) 405–409.

[12] D. Chen, Y. Wang, Y. Yu, Z. Hu, Crystallization and fluorescence properties of $Nd^{3+}$-doped transparent oxyfluoride glass–ceramics, Mater. Sci. Eng., B 123 (2005) 1–6.
[13] F. Xin, S. Zhao, S. Xu, G. Jia, D. Deng, H. Wang, L. Huang, Preparation and photoluminescence of Eu-doped oxyfluoride borosilicate glass–ceramics, J. Rare Earths 30 (2012) 6–9.
[14] B. Dieudonné, B. Boulard, G. Alombert-Goget, A. Chiasera, Y. Gao, S. Kodjikian, M. Ferrari, Up-down-conversion in $Yb^{3+}$–$Pr^{3+}$ co-doped fluoride glasses and glass–ceramics, J. Non-Cryst. Solids 377 (2013) 105–109.
[15] Y.J. Jung, K.H. Lee, T.H. Kim, Y.S. Kim, H.J. Chin, B.K. Ryu, Photoluminescence characterization for active structural glass composite; $SiO_2$–$B_2O_3$–ZnO doped $Mn^{2+}$ glass, J. Ceram. Process. Res. 10 (2009) 559–561.
[16] W. Stambouli, H. Elhouichet, B. Gelloz, M. Férid, Optical and spectroscopic properties of Eu-doped tellurite glasses and glass–ceramics, J. Lumin. 138 (2013) 201–208.
[17] Z. Pei, Y. Wang, D. He, X. Meng, Luminescence property of Eu-doped fluorochlorozirconate glass–ceramics, J. Rare Earths 27 (2009) 338–340.
[18] K. Linganna, M. Rathaiah, N. Vijaya, C. Basavapoornima, C.K. Jayasankar, S. Ju, W.T. Han, V. Venkatramu, 1.53 μm luminescence properties of $Er^{3+}$-doped K-Sr–Al phosphate glasses, Ceram. Int. 41 (2015) 5765–5771.
[19] P.Y. Shih, Thermal, chemical and structural characteristics of erbium-doped sodium phosphate glasses, Mater. Chem. Phys. 84 (2004) 151–156.
[20] H. Liu, R. Yang, Y. Wang, S. Liu, Influence of alumina additions on the physical and chemical properties of lithium-iron-phosphate glasses, Phys. Procedia 48 (2013) 17–22.
[21] J.R. Martinelli, F.F. Sene, L. Gomes, Synthesis and properties of niobium barium phosphate glasses, J. Non-Cryst. Solids 263–264 (2000) 263–270.
[22] S.K. Arepalli, H. Tripathi, V.K. Vyas, S. Jain, S.K. Suman, R. Pyare, S.P. Singh, Influence of barium substitution on bioactivity, thermal and physico-mechanical properties of bioactive glass, Mater. Sci. Eng., C 49 (2015) 549–559.
[23] J.E. Shelby, Introduction to Glass Science and Technology, second ed., Royal Society of Chemistry, Cambridge UK, 2005.
[24] K. Meyer, Characterization of the structure of binary zinc ultraphosphate glasses by infrared and Raman spectroscopy, J. Non-Cryst. Solids 209 (1997) 227–239.
[25] L. Popović, D. de Waal, J.C.A. Boeyens, Correlation between Raman wavenumbers and P–O bond lengths in crystalline inorganic phosphates, J. Raman Spectrosc. 36 (2005) 2–11.
[26] L. Khriachtchev, M. Räsänen, S. Novikov, L. Pavesi, Systematic correlation between Raman spectra, photoluminescence intensity, and absorption coefficient of silica layers containing Si nanocrystals, Appl. Phys. Lett. 85 (2004) 1511–1513.
[27] T.G.V.M. Rao, A. Rupesh Kumar, K. Neeraja, N. Veeraiah, M. Rami Reddy, Optical and structural investigation of $Eu^{3+}$ ions in $Nd^{3+}$ co-doped magnesium lead borosilicate glasses, J. Alloy. Compd. 557 (2013) 209–217.
[28] N. Vijaya, C.K. Jayasankar, Structural and spectroscopic properties of $Eu^{3+}$-doped zinc fluorophosphate glasses, J. Mol. Struct. 1036 (2013) 42–50.
[29] G. Blasse, A. Bril, W.C. Nieuwpoort, On the $Eu^{3+}$ fluorescence in mixed metal oxides: Part I—the crystal structure sensitivity of thr intensity ratio of electric and magnetic dipole emission, J. Phys. Chem. Solids 27 (1966) 1587–1592.
[30] C.E. Rodríguez-García, N. Perea-López, O. Raymond, G.A. Hirata, Photoluminescence properties of Eu-doped $LaSr_2AlO_5$, Sci. Adv. Mater. 4 (2012) 563–567.
[31] E.J. Sharp, M.J. Weber, G. Cleek, Energy transfer and fluorescence quenching in Eu– and Nd-doped silicate glasses, J. Appl. Phys. 41 (1970) 364–369.
[32] N.G. Boetti, D. Negro, J. Lousteau, F.S. Freyria, B. Bonelli, S. Abrate, D. Milanese, Spectroscopic investigation of $Nd^{3+}$ single doped and $Eu^{3+}$/$Nd^{3+}$ co-doped phosphate glass for solar pumped lasers, J. Non-Cryst. Solids 377 (2013) 100–104.